10-2020

Association of Liver Tissue Optical Properties and Thermal Damage

Vivek K. Nagarajan
Marquette University

Jerrold M. Ward
Global Vet Pathology

Bing Yu
Marquette University, bing.yu@marquette.edu

Lasers in Surgery and Medicine, Vol. 52, No. 8 (2020): 779-787. DOI.

Association of Liver Tissue Optical Properties and Thermal Damage

Vivek Krishna Nagarajan
Marquette University, Medical College of Wisconsin
Jerrold M. Ward
Global Vet Pathology
Bing Yu
Marquette University, Medical College of Wisconsin

Abstract

Background and Objectives

Complete thermocoagulation of tumors is vital to minimize the risk of local tumor recurrence after a thermal ablation. Histological assessments are not real-time and require experienced pathologists to grade the thermal damage (histopathology) [Correction added on 21 January, 2020 after first online publication: After thermal damage in the preceding sentence, (histopathology) was added]. Real-time assessment of thermal tissue damage during an ablation is necessary to achieve optimal tumor ablation. In our previous studies, we found that continuous monitoring of the wavelength-averaged (435–630 nm) tissue absorption coefficient (μ_a) and the reduced scattering coefficient (μ_s') during heating of a porcine liver at 100°C follows a sigmoidal growth curve. Therefore, we concluded that increases in the tissue μ_a and μ_s' during thermocoagulation were correlated with

true thermal damage. The goal of this study was to determine if increases in the tissue μ_a and μ_s' during thermocoagulation are correlated with true thermal damage.

Study Design/Materials and Methods

In this paper, continuously measured values of μ_a and μ_s' during heating of the porcine liver tissue were compared with the histology-assessed thermal damage scores at four different temperature points (37°C, 55°C, 65°C, and 75°C).

Results

The damage scores for the tissues in Group 3 (65°C) and Group 4 (75°C) were significantly different from each other and from the other groups. The damage scores were not significantly different between Group 1 (37°C) and Group 2 (55°C).

Conclusion

The results indicate that relative changes in μ_a and μ_s' can be used to classify thermal damage (histopathology) scores with an overall accuracy of 72.5% up to 75°C. [Correction added on 21 January, 2020 after first online publication: After thermal damage in the preceding sentence, (histopathology) was added]. Lasers Surg. Med. © 2019 Wiley Periodicals, Inc.

INTRODUCTION

Hepatocellular carcinoma (HCC) is the third most common cause of cancer-related deaths worldwide. In 2015, 854,000 new cases and 810,000 deaths related to HCC were reported worldwide. While surgery offers the best chance for a cure or prolonged survival, more than two-thirds of patients with primary liver cancer and 90% of patients with secondary liver cancer are inoperable because the tumors are close to or have invaded into major blood vessels, bile ducts, or other adjacent vital structures [1]. Thermal tissue ablation is a minimally invasive surgical procedure that is increasingly used to treat a variety of inoperable or unresectable tumors and tumor beds [2]. The increased sensitivity of tumor cells to heat is the basis for hyperthermia [3]. High-temperature hyperthermia (thermal ablation) is used to destroy cancerous tissue, for targeted tissue modification, and to remodel and reduce tumor masses [4]. In such ablative procedures, especially for ablating cancerous tissues, an inadequate amount of heat will lead to a partial ablation with an increased risk of local recurrences of the tumor [2]. On the other hand, an excessive thermal ablation of a tissue (normal or tumor) leads to undesirable effects, such as tissue charring, which complicate ablative procedures [2, 5-7]. Complete ablation rates after a single session of radio-frequency ablation (RFA), the most commonly used thermal ablation method for HCC treatment, vary from 48% to 97% [8-15]. The assessment of thermal damage is most commonly estimated by measuring the local tissue temperature and the duration of heating using the Arrhenius damage model [16]. Magnetic resonance thermometry (MRT) [17], computed tomography-based thermometry (CTT) [18, 19], and ultrasound thermometry [7, 20] (UST) have all been employed to quantify tissue temperatures noninvasively during thermal ablation procedures. MRT has been widely used for temperature mapping in conjunction with RFA [11], MWA, HIFU [21], and LITT (or laser ablation) [22] for monitoring ablation procedures. A temperature-based assessment of thermal damage is an indirect method. Therefore, a histological assessment of thermal damage remains the gold standard. However, a histological assessment is not real-time and requires experienced pathologists to grade the thermal damage. Real-time assessments of thermal tissue damage during ablation are necessary to achieve optimal tumor ablation [10, 14, 23-25]. Real-time monitoring of the tissue status during thermal ablation of tumors would significantly advance the state-of-the-art by ensuring complete destruction of tumor masses while avoiding tissue charring and excessive damage to normal tissues.

Quantitative diffuse reflectance spectroscopy (DRS) is a nondestructive method that can be used to quantify optical tissue properties *in vivo* [26-29]. Continuous optical monitoring of changes to optical tissue properties such as μ_a and μ_s' may be used for assessing tissue statuses during ablation procedures. A number of publications have reported differences in tissue absorption ($\mu_a(\lambda)$) and reduced scattering coefficients ($\mu_s'(\lambda)$) for native and coagulated tissues [30-37]. Studies that have measured the optical properties of native and coagulated porcine liver tissues have observed an increasing trend in $\mu_s'(\lambda)$ and $\mu_a(\lambda)$ [35, 38]. In particular, Ritz et al. [38] studied the changes to optical properties that occur after heating native tissues to different temperatures and concluded that the optical penetration depth significantly decreases during thermocoagulation. Spectra ratios have also been used to assess tissue coagulation [24, 25, 29, 39-41]. Hsu et al. [42] used visible light spectroscopy to identify the tumor margin and monitor the ablation to human livers *in vivo* and in cattle livers *ex vivo*. They reported that at higher temperatures, changes to the absorbance at 700 nm reaches a minimum (~95% decrease from the baseline at 79°C), which they claimed as an indicator of the end-point for protein denaturation. Buttemere et al. [40] studied the diffuse reflectance spectra from *in vivo* canine livers undergoing RFA and observed an overall increase in the DRS signal between 450 and 750 nm.

Decreased light penetration, increased light scattering and absorption, and/or an increase in tissue fluorescence have been some of the commonly reported findings in thermocoagulated tissues. However, a correlation between changes in optical tissue properties and the pathological status of tissue coagulation/damage during heating has not been established. Such a relationship may be used to predict the point of complete tissue ablation. Furthermore, the techniques used in the references [23, 30-37] are traditional methods for extracting μ_a and μ_s', which require tissue sectioning and/or an integrating sphere that are not applicable *in vivo*. The spectral ratios [24, 25, 29, 39-41] are subject to instrument drifts and movement artifacts, and the fluorescence-based methods [24, 33, 41] require complex and expensive hardware. Therefore, a robust and cost-effective system for determining optical tissue properties during a thermal ablation process is yet to be realized for a clinical setting. Investigating the relationship between relative changes in μ_a and μ_s' and the true thermal damage would help achieve a relatively cost-effective online ablation monitoring tool.

In our previous studies [43-45], we showed that the relative changes in μ_a and μ_s' of *ex vivo* porcine liver tissues follow a sigmoidal curve, which correlates well with the thermal damage calculated using the Arrhenius damage model. In this paper, relative changes in μ_a and μ_s' of porcine liver tissues are associated with histopathologically assessed thermal damage. Our hypothesis is that changes in μ_a and μ_s' are correlated with some specific pathological markers of thermal damage.

MATERIALS AND METHODS

DRS System

The integrated DRS system used in this paper has been illustrated in our previous paper [44]. In brief, the DRS system consists of a homemade needle-based fiber-optic probe, two visible-light spectrometers (Avantes BV, Apeldoorn, The Netherlands) with a white light-emitting diode (LED), one near-infrared (NIR) spectrometer with an 820 nm LED, and a laptop computer loaded with custom software. The fiber-optic probe includes two side-firing fibers (200/220 µm) spaced apart by 1 mm, a homemade extrinsic Fabry–Perot interferometric (EFPI) temperature sensor, and two forward-firing fibers (200/220 µm) for self-calibration [26, 27, 46] housed into an 18G Teflon tube, tipped with a 15 mm long 17G hypodermic needle (Fig. **1**). One of the two side-firing fibers is connected to the white LED to illuminate the target tissue and the other to the visible-light spectrometer A (Vis Spec A) for detecting the diffuse reflectance from the tissue. The self-calibration fibers loop the light from the white LED back to the visible-light spectrometer B (Vis Spec B) before it reaches the tissue using a diffusely reflective medium. The self-calibration records a calibration spectrum concurrent with the DRS measurement, which is used to correct for instrument fluctuations and probe bending losses [46].

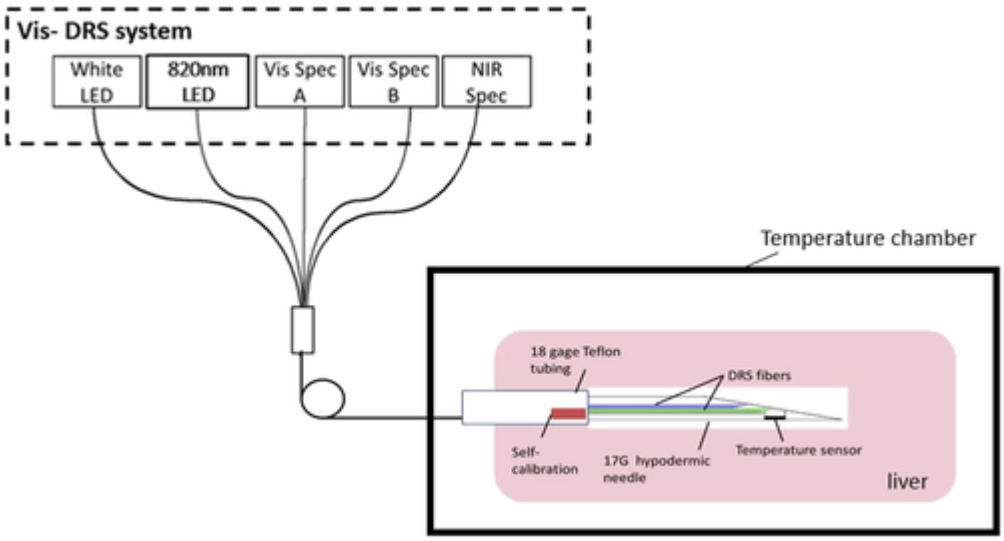

Figure 1 Schematic of the fiber-optic spectroscopic system, needle probe, and experimental setup. DRS, diffuse reflectance spectroscopy.

The EFPI sensor head was fabricated by laser fusion bonding two multimode fibers separated by a small air gap (L_c) to a borosilicate capillary tube with an outer diameter of 290 µm. The distance between the two bonding points, the gage length (L_g), is 2.0 mm. The EFPI sensor head is connected to the sensing arm of a 2 × 2 SM 50/50 fiber-optic coupler. The 820 nm LED was used to interrogate the EFPI sensor and the returned interferogram was collected by the NIR spectrometer (NIR Spec). The thermal expansion of borosilicate tubing alters the optical path difference between the two interfering waves that are reflected by the end-faces of the two fiber tips, shifting the peak positions of the interferogram. The temperature is determined by tracking the temperature-dependent wavelength shift in the interferogram. The temperature sensor was calibrated in a water bath and was found to have an accuracy of 1°C between 20°C and 95°C. A laptop computer with a custom LabVIEW program and embedded MATLAB scripts were used for instrument control, as well as data acquisition and analysis.

Sample Preparation

Fresh porcine liver tissues (from three pigs) were extracted immediately post-slaughtering from a local slaughterhouse and transported to the laboratory in an iced physiological saline solution. The average transport time was less than 30 minutes. Upon arrival, the liver was stored in a physiological saline solution at 4°C until use. The livers were cut into ~15 × 15 × 15 mm blocks (samples) for measurement. The tissue blocks were acquired from different sites on the liver to maximize the sample variability within each liver. Post-measurement treated tissue samples were cut into 4 × 2 mm blocks around the probe-tip and stored in a 10% neutral-buffered formalin solution for histopathological sectioning and analysis. All 40 tissue samples were used within 10 hours of procurement.

Optical Measurements

The 40 samples were randomly divided into four groups with 10 samples in each group. For each measurement, the needle probe was inserted into the center of the tissue sample, as illustrated in Figure **1**. After probe placement, the tissue samples were heated to preset temperatures. A thermal test chamber (Tenney Junior; Thermal Product Solutions, New Columbia, Pennsylvania; range: −75°C to 200°C with a uniformity of ±1°C) with interior dimensions of 16 × 11 × 11.8 and in-built controller for temperature settings was used to uniformly heat the tissue samples. The tissues diffuse reflectance and concurrent calibration spectrums, and the tissue temperature was continuously measured from the needle probe during the tissue heating. Prior to the tissue

heating, baseline measurements of native tissue samples were also obtained at room temperature. In Group 1, the tissue samples were heated to 37°C for 30 minutes (control). In Groups 2 and 3, the liver tissue samples were placed inside the temperature chamber (pre-heated to 100°C) until the tissue temperatures reached 55°C and 65°C, respectively. In Group 4, the liver tissue samples were heated in the 100°C chamber for 30 minutes. The duration of heating for Groups 2, 3, and 4 were 7.6 ± 0.7, 11 ± 1, and 30 minutes, respectively. After heating, the liver tissue samples around the probe-tip were cut into 4 × 2 mm blocks and placed in a 10% neutral-buffered formalin solution for histopathological analysis.

Data Analysis

Hemoglobin is the dominant chromophore in the visible spectrum. For our measurement, we extracted μ_a and μ_s' from the normalized diffuse reflectance spectrum using an inverse Monte Carlo model of diffuse reflectance [47]. The diffuse reflectance spectrum included many wavelengths. For all tissue samples, a baseline (native tissue) μ_a and μ_s' were recorded at room temperature prior to heating. The relative changes in μ_a and μ_s' were calculated as follows: $\frac{baseline-measured}{baseline}$. A one-way analysis of variance (ANOVA) (significance level = 0.05) was used to study the variations in μ_a and μ_s' (absolute and relative) among the four groups. The tissue samples acquired from the livers of the three pigs were assigned randomly to G1–4. The sample dependency has not been considered for analysis. In addition, CEM43 (cumulative equivalent minutes at 43°C) calculated using the duration of heating and tissue temperature data is compared with the changes in the measured tissue optical properties [48]. The CEM43 model converts all thermal exposures to equivalent minutes at 43°C. The same dose concept can be used to quantify thermal exposure during tissue heating. The gross histopathological analysis was performed on all tissue samples using 4 µm hematoxylin and eosin (H&E) stained sections. The histopathologist was blinded to the treatment groups, and only the samples in the control group (Group 1) were identified for the pathologist. The sequence of tissue-level changes during tissue heating are listed in Table **1**. Pathological markers, such as hepatocyte nuclei shrinking, presence of small and large vacuoles, portal inflammation, and collagen bluing were observed from H&E images by gross examination. For each sample, the extent of hepatocyte nuclei shrinking and collagen bluing were used to determine the overall thermal tissue damage. The histopathologically assessed thermal damage was graded on a scale of 0–4 (0—normal, 1—minimal, 2—mild, 3—moderate, 4—severe), based on the overall changes in hepatocytes, collagen bluing, and nuclei shrinking. A one-way ANOVA, along with Tukey's test (significance level = 0.05), was used to study the variations in the histopathologically assessed thermal damage scores between the sample groups.

Table 1. Sequence of Events During Thermal Denaturation of Biological Tissues, Modified from Thomsen et al. [49]

Temperature (°C)	Histopathologic effects due to thermal heating
40–43	Deactivation of enzymes: Reversible damage to cells
>43	Membrane rupture
	Cell shrinkage and hyperchromasia
	Enzyme denaturation: Cell death
>58	Hyalinization of collagen
69–75	Birefringence loss

Linear discriminant analysis was used to group the relative changes in μ_a and μ_s' and the overall thermal damage scores. An in-built MATLAB classification toolbox was used to determine the implicit functions describing the discriminant line between each group, as shown in Table **3**a, with the true and false positive rates shown in Table **3**b.

RESULTS

Liver Tissue Experiment

The absolute and relative changes in the tissues' μ_a and μ_s' between the tissue groups are presented in Figure **2** and Table **2**. As shown in Figure **2**a and c, the absolute and relative changes to μ_a in Group 3 were significantly different from Group 1 ($P < 0.0001$) and Group 2 ($P < 0.013$), but no significant difference was observed between Group 1 and Group 2 ($P = 0.6$ (absolute) and $P = 0.06$ (relative) changes). The absolute and relative changes in tissue μ_a for Groups 3 and 4 were significantly different from each other ($P < 0.0001$). In Figure **2**b and d, the absolute and relative changes in μ_s' were significantly different between Groups 1 and 2 ($P < 0.05$), between Groups 1 and 3 ($P < 0.013$), and between Groups 2 and 3 ($P < 0.0001$). The absolute and relative changes in μ_s' were also significantly different between Groups 3 and 4 ($P < 0.01$). Unlike Groups 1–3, the tissue samples in Group 4 did not have a set temperature point and the end-tissue temperature for Group 4 varied from 74°C to 85°C at the probe-tip. The absolute and relative changes in tissue μ_a and μ_s' for Group 4 were not significantly different from Groups 1–2 ($P > 0.05$).

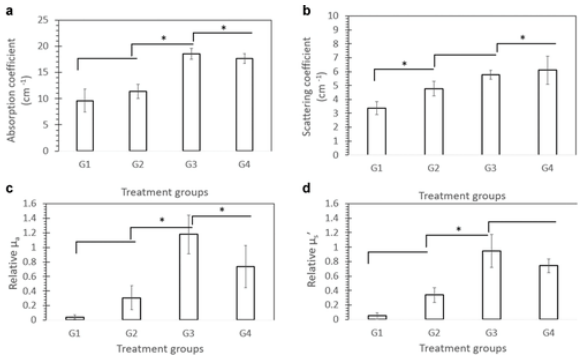

Figure 2 Liver tissues' μ_a and μ_s' for each group: (**a** and **b**) absolute and (**c** and **d**) relative changes. (*$P < 0.05$).

Table 2. Mean Damage Scores and Optical Properties for the Liver Tissue Samples

Marker	Group 1 (n = 10)	Group 2 (n = 10)	Group 3 (n = 10)	Group 4 (n = 10)
Overall hepatic changes	0	0.1 ± 0.2	1.3 ± 0.4	2.5 ± 0.3
Hepatocyte nuclei shrinking	0	0.7 ± 0.3	0.9 ± 0.2	1
Collagen bluing	0	0	1.3 ± 0.4	2.6 + 0.3
μ_a (cm^{-1})	3.4 ± 1	4.8 ± 1	5.8 ± 0.6	6.1 ± 1.8a
μ_s' (cm^{-1})	9.6 ± 4.4	11.3 ± 2.7	18.6 ± 2.1	16.5 ± 3.1a
Relative μ_a	0.05 ± 0.09	0.34 ± 0.2	0.95 ± 0.46	0.74 ± 0.2a
Relative μ_s'	0.04 ± 0.06	0.31 ± 0.32	1.2 ± 0.53	0.74 ± 0.6a

The thermal damage scoring scheme was as follows: 0—normal, 1—minimal, 2—mild, 3—moderate, and 4—severe.

[a] Measurements reported at 75°C.

A representative H&E image of the liver tissue sections from each group is shown in Figure **3**a. The damage scores from the histological report are listed in Table **2**. None of the samples had a damage score of 4 (severely damaged). The highest level of damage for all samples was observed in Group 4, with an overall damage score of 3 (moderately damaged). The mean scores for the overall hepatic changes in Groups 1–4 were 0, 0.1 ± 0.3, 1.3 ± 0.7, and 2.5 ± 0.5, respectively. The overall hepatic changes for Groups 3–4 were significantly different from Group 1 ($P < 0.02$) and from each other ($P < 0.0001$), as shown in Figure **3**b. However, the overall hepatic changes in Groups 1 and 2 were not significantly different ($P = 0.81$). The mean scores for hepatocyte nuclei shrinking in Groups 1–4 were 0, 0.7 ± 0.5, 0.9 ± 0.3, and 1, respectively. The nuclei shrinking in Groups 2, 3, and 4

were significantly different from Group 1 ($P < 0.0001$), but no significant difference was found between Groups 2 and 3 ($P = 0.08$) and between Groups 3 and 4 ($P = 0.61$). Collagen bluing in Groups 1–4 were significantly different from each other ($P < 0.04$), which was visually observed by gross examination only in Groups 3 and 4. The mean scores for collagen bluing in Groups 3 and 4 were 1.3 ± 0.4 and 2.6 ± 0.3, respectively, which were significantly different ($P < 0.0001$) from each other and from all other groups.

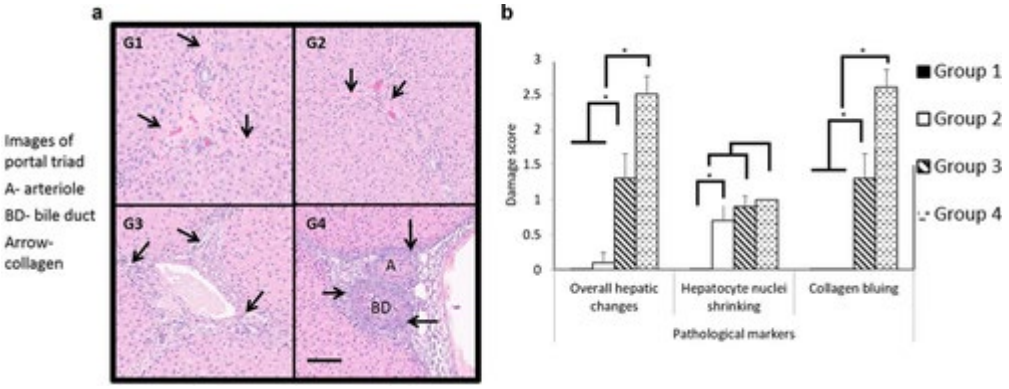

Figure 3 (**a**) Hematoxylin and eosin image of a portal triad showing collagen bluing in each group (black arrows). (**b**) Comparison of the group mean scores for each pathological marker. Scale bar = 300 µm. G1 (37°C), G2 (55°C), G3 (65°C), G4 (75°C). A, arteriole; BD, bile duct.

The results show that relative changes in μ_a and μ_s' can be used to classify thermal damage scores with an overall accuracy of 72.5%. From a discriminant analysis, all samples were correctly classified into their original groups with an accuracy of 72.5%, as shown in Table **3**, using the relative changes in μ_a, μ_s', and the overall damage scores. The implicit functions describing the discriminant line between the two groups are also provided in Table **3**. The accuracy of classification in Groups 1–4 using the relative changes in μ_a, μ_s', and the overall damage scores were 90%, 60%, 50%, and 80%, respectively.

Table 3. Linear Discriminant Analysis was Used to Group the Relative Changes in μ_a, and μ_s', and the Overall Thermal Damage Scores

3a

Coefficients of implicit functions describing boundaries between groups *f*: (k +Rel. μ_s' * *x*1 + Rel. μ_a * *x*2 + Thermal damage score * *x*3) = 0				
Groups	K [constant]	Rel. μ_s' [ratio]	Rel. μ_a [ratio]	Thermal damage score
1 vs 2	0.7872	-2.6988	-1.0256	0.0964
1 vs 3	8.4580	-7.5258	-2.5712	-4.6826
1 vs 4	16.0047	-4.8919	0.4782	-11.36
2 vs 3	7.6708	-4.8270	-1.5456	-4.779
2 vs 4	15.2175	-2.1931	1.5038	-11.4564
3 vs 4	7.5467	2.6338	3.0495	-6.6774

3b

True Class	G1	90%	10%		
	G2	30%	60%	10%	
	G3		30%	50%	20%
	G4			20%	80%
		G1	G2	G3	G4

		Predicted class using table 3 (b) discriminant functions			

90%	10%
60%	40%
50%	50%
80%	20%
True Positive Rate	False Positive Rate

The resulting implicit functions, as shown in Table 3a, were used to predict the thermal damage scores of the measured relative values of μ_a and μ_s'. The accuracy of such a prediction is shown in Table 3b. Optical tissue properties at 75°C were used to represent Group 4 in the following analysis.

DISCUSSION

In this paper, a fiber-optic spectroscopic system with a miniature needle probe was used to continuously monitor *T*, μ_a, and μ_s' during the heating of *ex vivo* porcine liver tissues.

The μ_a and μ_s' for native *ex vivo* liver tissues at room temperature were 9.6 ± 3.7 and 3.5 ± 0.9 cm^{-1}, respectively. The liver tissue samples in each group were exposed to different thermal dosages. In general, the optical tissue properties increased for all tissue samples during heating [44]. Therefore, we explored the feasibility of using μ_a and μ_s' to identify the tissue statuses at different stages of heating. The continuous changes in μ_a and μ_s' were categorized into four levels of thermal damage, Groups 1–4. It was found that large variations in the absolute μ_a and μ_s' observed in Figure **2**a and b showed poor contrast, which makes it difficult to identify different groups with certainty. For an *ex vivo* tissue, multiple factors, such as loss of blood flow, tissue handling, mechanical damage, dehydration, and accumulation of absorptive fluids within the tissue sample, may have resulted in such large variations in the baseline of μ_a and μ_s'. The samples in Group 1 acted as a negative control in this study, as they were exposed to 37°C for 30 minutes, partially accounting for the tissue dehydration within the thermal chamber. Future studies may be performed in a water heating bath. In our previous papers [43, 44], we have shown that the relative changes in μ_a and μ_s' have a better contrast than the absolute μ_a and μ_s' values. The relative changes in μ_a for Groups 3 and 4 were significantly different from each other ($P = 0.003$) (Fig. **2**a and c). However, no significant difference was observed between Groups 1 and 2 ($P = 0.2$) for the relative changes in μ_a. Analogously, the relative changes in μ_a correlate well with the overall hepatocyte changes and collagen bluing, as shown in Figure **3**b. The mean damage scores for hepatocyte nuclei shrinkage were significantly different for Groups 1 and 2 ($P < 0.0001$), but not differentiable in Groups 3 and 4 ($P = 0.61$). However, Groups 3 and 4 had significantly different mean scores for collagen bluing and overall hepatic changes.

The relative changes in μ_a and μ_s' still had large variations and Group 4 was not significantly different from Groups 1 and 2. Unlike Groups 2 and 3, the tissue samples in Group 4 did not have a set temperature point. The end-tissue temperature for Group 4 varied from 74°C to 85°C, resulting in sampling the tissue status at varying levels of thermal damage and thus larger variations in the measured μ_a and μ_s' (Fig. **2**). Therefore, for Group 4, only μ_a and μ_s' at 75°C were compared with Groups 1–3, as seen in Figure **4**. The variations in μ_a and μ_s' were far smaller at 75°C than in Group 4. The relative changes in μ_a and μ_s' at 75°C were significantly different from Groups 1 and 2 ($P < 0.003$), and not significantly different from Group 3. Interestingly, the relative changes to μ_a in Group 3 were significantly different from Groups 1, 2, and 4 ($P < 0.003$), implying that the relative change in μ_a may have a peak region in Group 3, possibly due to the aggregation of chromophores [50].

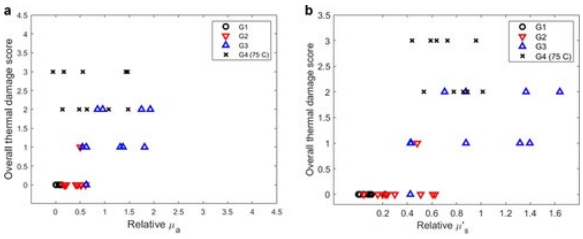

Figure 4 Overall damage scores and relative changes in (a) μa and (b) μ_s'. μa and μ_s' for G4 are replaced with μa and μs' at 75°C.

The discrepancy when comparing μ_a and μ_s' at 75°C and the mean damage scores for Group 4 (in which the samples might have been heated beyond 75°C) needs further investigation. In our previous study [43, 44], we observed that the onset of plateauing for continuous changes in μ_a and μ_s' during tissue heating occurred at ~67°C. It is unclear which pathological marker caused plateauing, but the initiation of collagen denaturation might be the reason. Bozec et al. [51] observed the onset of collagen denaturation at 58 ± 10°C and gelatinization at 65 ± 10°C. Furthermore, Bozec et al. reported that the periodicity of striations decreased in denatured collagen from 67 to 38 nm. The striations in collagen tissues are optical scatterers [52]. Hence, a reduction in the periodicity of striations in collagen tissue would tend to increase μ_s'. Collagen bluing, which is usually observed in denatured collagen (Groups 3 and 4), is a specific pathological marker for thermal denaturation [53, 54]. The bluing of collagen due to thermal denaturation is observable from Group 3 onwards, and bluing increases in Group 4, as seen in Figure **3**a. The mean scores for collagen bluing in Groups 3 and 4 were 1.3 ± 0.4 and 2.6 ± 0.3, respectively, which were significantly different ($P < 0.0001$) from each other and from all other groups. Furthermore, CEM43 > 80 min can cause minor thermal damage to the liver tissues during local heating [55]. Seror et al.[56] showed that CEM43 = 320 min is sufficient enough to cause thermal coagulation in pig livers. In our study, CEM43 for samples in Groups 1–3, at 75°C and Group 4 were 8.7×10^{-10}, 3.1×10^{04}, 4.6×10^{07}, 8.6×10^{10}, and 2.7×10^{12} minutes, respectively, as shown in Figure **5**. This indicates the presence of thermal tissue damage in Groups 2–4 and at least a three-order increase in the thermal dosage for each successive group.

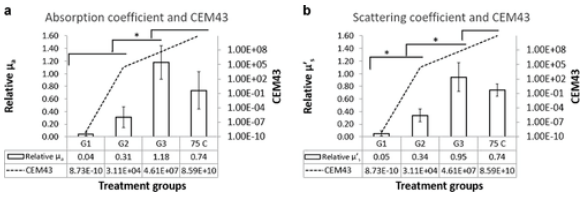

Figure 5 Comparison between CEM43 and relative changes in (a) μ_a and (b) μ_s'. μ_a and μ_s' for G4 are replaced with μ_a and μ_s' at 75°C.

The relative changes of μ_s' in Groups 3 and 4 (75°C) are not differentiable based on the magnitude alone. To differentiate Groups 3 and 4, the relative changes (magnitude) along with the duration of heating, may be used to estimate the tissue damages in real-time. Ritz et al.[38] heated the liver tissues to 80°C for 20 min to achieve complete denaturation. It is unclear if any of the samples in our study were completely denatured. Nevertheless, the temperature point 75°C occurs at 20 ± 6 min, which is midway between Group 3 (11 ± 1 min) and Group 4 (30 min), and is similar to the heating duration observed by Ritz et al.[38].

Our long-term goal is to achieve a portable integrated laser-ablation tool with real-time thermal damage monitoring. In this paper, we have shown that the fiber optic spectroscopic system may be used as a cost-effective portable tool for continuously monitoring the thermal tissue damage during heating. The use of *ex vivo* noncancerous liver tissue prevented us from measuring the full extent of thermal damage (including the primary and secondary effects). The histologically assessed damage reported in this paper is primarily qualitative and insensitive to low thermal damages. In future studies, we plan to explore more sensitive damage and use a

finer quantitative method such as birefringence loss targeting heat shock proteins (HSP 70) [57] and collagen-specific stains such as Sirius-red [58] and Masson's trichrome [59] to determine the status of pathological markers. Nevertheless, we have shown that the relative changes in μ_s' serve as a good marker for differentiating the three levels of thermal damage (Groups 1, 2, 3, and 4). The decrease in the relative μ_s' for Group 4 needs to be investigated in future studies. The impact of hyalinization of collagen, chromophore denaturation, and subsequent tissue denaturation at higher thermal doses (longer exposure at lower temperatures) needs to be investigated to understand the limitations of optical monitoring of thermal tissue damage. Nevertheless, the results from this study warrant studying the full extent of thermal damage using longitudinal animal studies to capture the primary and secondary effects of thermal injury.

CONCLUSION

In conclusion, a fiber-optic spectroscopic system with an integrated probe was used to collect the DRS measurements at four different temperature points. The histopathology of heated liver tissues was used to assess the true thermal tissue damage at each temperature point. Results show that the relative changes in μa and μ_s' can be used to classify the thermal damage scores with an overall accuracy of 72.5% at temperatures up to 75°C. More specifically, the accuracy of classification in Groups 1–4 (75°C) using relative changes in μa, μ_s', and the overall damage scores were 90%, 60%, 50%, 80%, respectively. It is unclear if differentiating the thermal damage up to 75°C is enough for a real-time thermal damage assessment. Nevertheless, we have shown that changes in optical properties can be correlated to thermal denaturation.

ACKNOWLEDGMENTS

The study was supported by a Marquette University startup grant to Dr. B. Yu.

References

Forner AL, Bruix JM, J. Hepatocellular carcinoma. *Lancet* 2012; 379:1245-1255.

Chu KF, Dupuy DE. Thermal ablation of tumours: Biological mechanisms and advances in therapy. *Nat Rev Cancer* 2014; 14:199-208.

Cavaliere R, Ciocatto EC, Giovanella BC, et al. Selective heat sensitivity of cancer cells. Biochemical and clinical studies. *Cancer* 1967; 20:1351-1381.

Diederich CJ. Thermal ablation and high-temperature thermal therapy: Overview of technology and clinical implementation. *Int J Hyperthermia* 2005; 21:745-753.

Sturesson C. Interstitial laser-induced thermotherapy: influence of carbonization on lesion size. *Lasers Surg Med* 1998; 22:51-57.

Janda P, Sroka R, Mundweil B, Betz CS, Baumgartner R, Leunig A. Comparison of thermal tissue effects induced by contact application of fiber guided laser systems. *Lasers Surg. Med.* 2003; 33:93-101.

Varghese T, Zagzebski JA, Chen Q, et al. Ultrasound monitoring of temperature change during radiofrequency ablation: preliminary in-vivo results. *Ultrasound Med Biol* 2002; 28:321-329.

Chen MS, Li JQ, Zheng Y, et al. A prospective randomized trial comparing percutaneous local ablative therapy and partial hepatectomy for small hepatocellular carcinoma. *Ann Surg* 2006; 243:321-328.

Curley SA, Izzo F, Ellis LM, Nicolas Vauthey J, Vallone P. Radiofrequency ablation of hepatocellular cancer in 110 patients with cirrhosis. *Ann Surg* 2000; 232:381-391.

Hori T, Nagata K, Hasuike S, et al. Risk factors for the local recurrence of hepatocellular carcinoma after a single session of percutaneous radiofrequency ablation. *J Gastroenterol* 2003; 38:977-981.

Livraghi T, Goldberg SN, Lazzaroni S, et al. Hepatocellular carcinoma: Radio-frequency ablation of medium and large lesions. *Radiology* 2000; 214:761-768.

Livraghi T, Goldberg SN, Lazzaroni S, Meloni F, Solbiati L, Gazelle GS. Small hepatocellular carcinoma: treatment with radio-frequency ablation versus ethanol injection. *Radiology* 1999; 210:655-661.

Llovet JM, Vilana R, Bru C, Bianchi L, Salmeron JM, Boix L, et al. Increased risk of tumor seeding after percutaneous radiofrequency ablation for single hepatocellular carcinoma. *Hepatology* 2001; 33:124-1129

Poon RT, Ng KK, Lam CM, Ai V, Yuen J, Fan ST. Effectiveness of radiofrequency ablation for hepatocellular carcinomas larger than 3cm in diameter. *Arch Surg* 2004; 139:281-287.

Raut CP, Izzo F, Marra P, et al. Significant long-term survival after radiofrequency ablation of unresectable hepatocellular carcinoma in patients with cirrhosis. *Ann Surg Oncol* 2005; 12:616-628.

Arrhenius S. Über die Reaktionsgeschwindigkeit bei der Inversion von Rohrzucker durch Säuren. *Z Phy Chem* 1889; 4:226-248.

Vogl TJ, Huebner F, Naguib NNN, et al. MR-based thermometry of laser induced thermotherapy: temperature accuracy and temporal resolution in vitro at 0.2 and 1.5 T magnetic field strengths. *Laser Surg Med* 2012; 44:257-265.

Schena E, Saccomandi P, Giurazza F, et al. Experimental assessment of CT-based thermometry during laser ablation of porcine pancreas. *Phys Med Biol* 2013; 58:5705-5716.

Bruners P, Levit E, Penzkofer T, et al. Multi-slice computed tomography: A tool for non-invasive temperature measurement? *Int J Hyperthermia* 2010; 26:359-365.

Lewis MA, Staruch RM, Chopra R. Thermometry and ablation monitoring with ultrasound. *Int J Hyperthermia* 2015; 31:163-181.

Jenne JW, Preusser T, Gunther M. High-intensity focused ultrasound: Principles, therapy guidance, simulations, and applications. *Z Med Phys* 2012; 22:311-322.

Rosenberg C, Hoffman COM, Mensel B, Puls R, Hosten N. Laser ablation. *Radiology* 2012; 52:15-21.

Adams MT, Wang Q, Cleveland RO, Roy RA. Thermal dose dependent optical property changes of ex vivo chicken breast tissues between 500 and 1100 nm. *Phys Med Biol* 2014; 59:3249-3260.

Anderson CD, Lin WC, Beckham J, et al. Fluorescence spectroscopy accurately detects irreversible cell damage during hepatic radiofrequency ablation. *Surgery* 2004; 136:524-531.

Hsu CP, Razavi MK, So SK, Parachikov IH, Benaron DA. Liver tumor gross margin identification and ablation monitoring during liver radiofrequency treatment. *J Vasc Interv Radiol* 2005; 16:1473-1478.

Yu B, Shah A, Nagarajan VK, Ferris DG. Diffuse reflectance spectroscopy of epithelial tissue with a smart fiber-optic probe. *Biomed Opt Express* 2014; 5:675-689.

Yu B, Nagarajan VK, Ferris DG. Mobile fiber-optic sensor for detection of oral and cervical cancer in the developing world. *Methods Mol Biol* 2015; 1256:155-170.

Yu B, Lo JY, Kuech TF, Palmer GM, Bender JE, Ramanujam N. Cost-effective diffuse reflectance spectroscopy device for quantifying tissue absorption and scattering in vivo. *J Biomed Opt* 2008; 13:060505

Tanis E, Spliethoff JW, Evers DJ, et al. Real-time in vivo assessment of radiofrequency ablation of human colorectal liver metastases using diffuse reflectance spectroscopy. *Eur J Surg Oncol* 2016; 42:251-259.

Hafeez-Ullah U, Atif M, Firdous S, et al. Optical properties of normal and thermally coagulated chicken liver tissue measured ex-vivo with diffuse reflectance. *Opt Spectrosc* 2011; 110:313-319.

Dressler C, Schwandt D, Beuthan J, Mildaziene V, Zabarylo U, Minet O. Thermally induced changes of optical and vital parameters in human cancer cells. *Laser Phys Lett* 2010; 7:817-823.

Wei HJ, Xing D, He BH, et al. [Thermal coagulation of human benign prostatic hyperplasia tissues induced changes in the absorption and scattering properties in spectral range from 590 to 1064 nm in vitro]. *Guang Pu Xue Yu Guang Pu Fen Xi* 2008; 28:394-398.

Schwarz RA, Gao W, Daye D, Williams MD, Richards-Kortum R, Gillenwater AM. Autofluorescence and diffuse reflectance spectroscopy of oral epithelial tissue using a depth-sensitive fiber-optic probe. *Appl Opt* 2008; 47:825-834.

Holmer C, Lehmann KS, Risk J, et al. Colorectal tumors and hepatic metastases differ in their optical properties-relevance for dosimetry in laser-induced interstitial thermotherapy. *Lasers Surg Med* 2006; 38:296-304.

Terenji A, Willmann S, Osterholz J, Hering P, Schwarzmaier HJ. Measurement of the coagulation dynamics of bovine liver using the modified microscopic Beer-Lambert Law. *Lasers Surg Med* 2005; 36:365-370.

Swartling J, Palsson S, Platonov P, Olsson SB, Andersson-Engels S. Changes in tissue optical properties due to radio-frequency ablation of myocardium. *Med Biol Eng Comput* 2003; 41:403-409.

Yaroslavsky AN, Schulze PC, Yaroslavsky IV, Schober R, Ulrich F, Schwarzmaier HJ. Optical properties of selective native and coagulated human brain tissues in vitro in the visible and near infrared spectral range. *Phys Med Biol* 2002; 47:2059-2073.

Ritz JP, Roggan A, Isbert C, Muller G, Buhr HJ, Germer CT. Optical properties of native and coagulated porcine liver tissue between 400 and 2400 nm. *Lasers Surg Med* 2001; 29:205-212.

Yoshimura H, Viator JA, Jacques SL. Relationship between damaged fraction and reflected spectra of denaturing tissues. *Lasers Surg Med* 2005; 37:308-313.

Buttemere CR, Chari RS, Anderson CD, Washington MK, Mahadevan-Jansen A, Lin WC. In vivo assessment of thermal damage in the liver using optical spectroscopy. *J Biomed Opt* 2004; 9:1018-1027.

Lin WC, Buttemere C, Mahadevan-Jansen A. Effect of thermal damage on the in vitro optical and fluorescence characteristics of liver tissues. *IEEE J Sel Top Quantum Electron* 2003; 9:162-170.

Hsu CP, Razavi MK, So SK, Parachikov IH, Benaron DA. Liver tumor gross margin identification and ablation monitoring during liver radiofrequency treatment. *J Vasc Interv Radiol* 2005; 16:1473-1478.

Nagarajan VK, Gogineni VR, White SB, Yu B. Changes in optical properties during heating of ex vivo liver tissues. IN *SPIE BiOS*; 2017: p.7.

Nagarajan VK, Gogineni VR, White SB, Yu B. Real time evaluation of tissue optical properties during thermal ablation of ex vivo liver tissues. *Int J Hyperthermia* 2019; 35:176-182.

Nagarajan VK, Yu B. Monitoring of tissue optical properties during thermal coagulation of ex vivo tissues. *Lasers Surg Med* 2016; 48:686-694.

Yu B, Fu HL, Ramanujam N. Instrument independent diffuse reflectance spectroscopy. *J Biomed Opt* 2011; 16:011010.

Palmer GM, Ramanujam N. Monte Carlo-based inverse model for calculating tissue optical properties. Part I: Theory and validation on synthetic phantoms (vol 45, pg. 1062, 2006). *Appl Opt* 2007; 46:6847.

Sapareto SA, Dewey WC. Thermal dose determination in cancer therapy. *Int J Radiat Oncol, Biol, Phys* 1984; 10:787-800.

Thomsen S. Pathologic analysis of photothermal and photomechanical effects of laser-tissue interactions. *Photocem Photobiol* 1991; 53:825-835.

Nilsson AM, Sturesson C, Liu DL, Andersson-Engels S. Changes in spectral shape of tissue optical properties in conjunction with laser-induced thermotherapy. *Appl Opt* 1998; 37:1256-1267.

Bozec L, Odlhya M. Thermal denaturation studies of collagen by microthermal analysis and atomic force mocroscopy. *Biophys J* 2011; 101:228-236.

Saidi IS, Jacques SL, Tittel FK, Mie and Rayleigh modeling of visible-light scattering in neonatal skin. *Appl Opt* 1995; 34:7410-7418.

Majaron B, Srinivas SM, Huang H, Nelson JS. Deep coagulation of dermal collagen with repetitive Er:YAG laser irradiation. *Lasers Surg Med* 2000; 26:215-222.

Ruidiaz ME, Cortes-Mateos MJ, Sandoval S, et al. Quantitative comparison of surgical margin histology following excision with traditional electrosurgery and a low-thermal-injury dissection device. *J Surg Oncol* 2011; 104:746-754.

Yarmolenko PS, Moon EJ, Landon C, et al. Thresholds for thermal damage to normal tissues: an update. *Int J Hyperthermia* 2011; 27:320-343.

Seror O, Lepetit-Coiffé M, Le Bail B, de Senneville BD, Trillaud H, Moonen C, Quesson B. Real time monitoring of radiofrequency ablation based on MR thermometry and thermal dose in the pig liver in vivo. *Eur Radiol*2008; 18:408-416.

Flanagan SW, Ryan AJ, Gisolfi CV, Moseley PL. Tissue-specific HSP70 response in animals undergoing heat stress. *Am J Physiol* 1995; 268:R28-R32.

Segnani C, Ippolito C, Antonioli L, et al. Histochemical detection of collagen fibers by Sirius Red/Fast Green is more sensitive than van Gieson or Sirius Red alone in normal and inflamed rat colon. *PLoS One* 2015; 10. e0144630.

Chvapil M, Speer DP, Owen JA, Chvapil TA. Identification of the depth of burn injury by collagen stainability. *Plast Reconstr Surg* 1984; 73:438-441.